EPTT 2024
Escola de Primavera de Transição e Turbulência

ABCM
Associação Brasileira de Engenharia e Ciências Mecânicas

EPTT-2024-0037
Influence of the bed slope on axisymmetric gravity current propagation

Sara Mata
Guilherme Fuhrmeister Vargas
Karina Ruschel
Pontifical Catholic Rio Grande do Sul University
sara.sosa85@edu.pucrs.br
vargas.guilherme@edu.pucrs.br
karina.ruschel@pucrs.br

Abstract. *Gravity currents can occur in the ocean due to underwater landslides and play a critical role in sediment transport. The focus of this study is to characterize the influence of bed slope on the propagation of axisymmetric gravity currents. The research focuses on analyzing the front velocity, turbulent structures, and the potential formation of hydraulic jumps. The findings highlight the influence of bed slope on the spreading dynamics, the size and intensity of turbulent structures, and the conditions leading to hydraulic jumps. The results are based on numerical simulations, which are made possible by the resources provided by PUCRS High Performance Laboratory. This research is funded by Petrobras.*

Keywords: *Density current, axisymmetric configuration, turbulent structures, bed slope, Froude number*

1. INTRODUCTION

Density currents are gravity-driven flows caused by differences between the current and the surrounding environment. The higher density of the fluid currents can be attributed to salinity, temperature, or suspended particles. In the ocean, density currents are often triggered by underwater landslides on the continental shelf or at a river mouth. These currents are responsible for transporting sediment across vast distances, sometimes reaching abyssal depths (Mulder and Alexander, 2001), where sedimentary deposits are formed.

Mathematical models have been developed to describe the mechanisms of sediment transport and deposition in density currents. These models are based on turbulent structures and on the density current propagation velocity measured in the field in various locations around the globe (Kuenen and Menard, 1952; Sylvester *et al.*, 2011; Azpiroz-Zabala *et al.*, 2017; Dorrell *et al.*, 2015). However, much remains unknown about the nature and properties of natural density currents due to the difficulty in measuring sediment concentration on a real scale (Talling *et al.*, 2015).

The experiments developed in the laboratory represent the dynamics of the phenomenon on a smaller scale. A canonical example, with a fixed initial volume (Simpson, 1999; Bonnecaze *et al.*, 1995; Ross *et al.*, 2002), consists of the release of a dense fluid into a less dense ambient fluid in steady state, submerged in a closed reservoir.

In this sense, highly resolved three-dimensional numerical modeling (Härtel *et al.*, 2000; Cantero *et al.*, 2007; Espath *et al.*, 2015; Schuch *et al.*, 2018; Frantz *et al.*, 2021; Farenzena, 2021) reproduces the physical quantities provided by experiments, thus adding information that is not possible to record with measuring instruments, such as turbulent structures present at the interface between the current and the ambient fluid (Kneller *et al.*, 1999; Dubief and Delcayre, 2000; Cantero *et al.*, 2008; Francisco *et al.*, 2017; Dai and Huang, 2022; Vianna *et al.*, 2022).

The axisymmetric configuration, characterized by the height and radius of the initial volume in unconfined propagation, characterizes situations such as landslides or dredging on a sloping boundary, where it is interesting to know the bed slope influence in the mixing process.

Zgheib *et al.* (2016) detected a converging flow towards the center of the current due to the finite volume of the release on a uniform slope. This phenomenon induces a second acceleration phase in the front velocity of the current. Based on these findings, the present work aims to characterize the turbulent structures generated by the dynamics of the gravity currents propagating down a bed slope.

2. METHODOLOGY

2.1 Mathematical equations

In order to simulate the conservative density current, the continuity equation, the Navier-Stokes equation and the scalar concentration transport equation are applied in the axisymmetric lock-release configuration, with a bed slope. In this configuration, for the initial time instant, the fluid with the highest density (ρ_1) is confined in the cylinder of height L_2 and radius r_0, separated from the ambient fluid with the lowest density (ρ_0) (Figure 1).

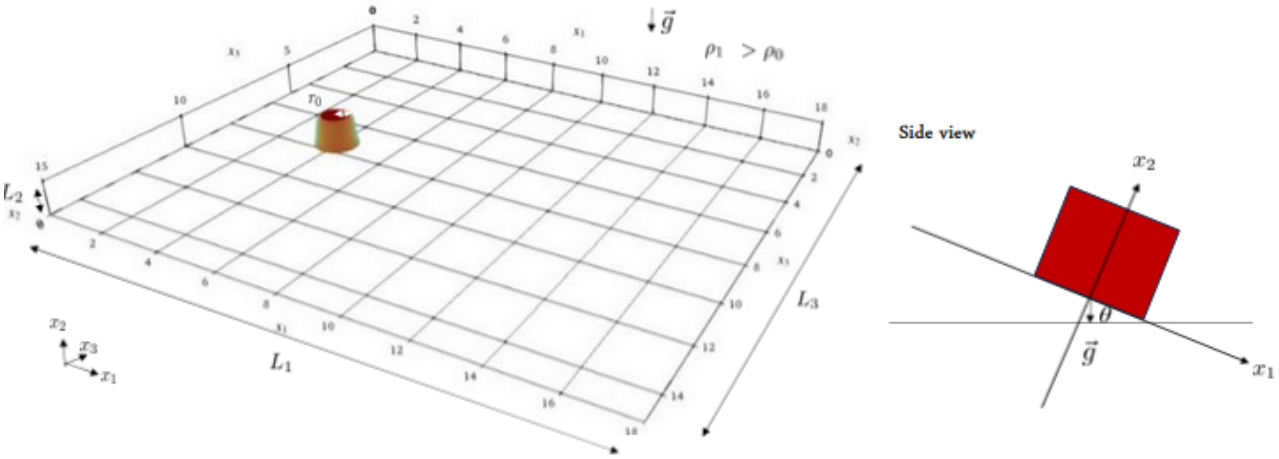

Figure 1. Initial configuration

The dimensionless mathematical equations that describe the problem, in the Boussinesq approximation for a conservative current, have the following form:

$$\frac{\partial u_i}{\partial x_i} = 0 \tag{1}$$

$$\frac{\partial u_i}{\partial t} + u_j \frac{\partial u_i}{\partial x_j} = -\frac{\partial P}{\partial x_i} + \frac{1}{Re}\frac{\partial^2 u_i}{\partial x_j \partial x_j} - \varphi \hat{e}^g \tag{2}$$

$$\frac{\partial \varphi}{\partial t} + u_j \frac{\partial \varphi}{\partial x_j} = \frac{1}{ReSc}\frac{\partial^2 \varphi}{\partial x_j \partial x_j} \tag{3}$$

where u_i, P and φ correspond to the unknowns variables of the problem, being the velocity vector, pressure and scalar concentration, respectively. Eqs. 1, 2, 3 were dimensionless with the scale velocity $U_b = \sqrt{Hg(\rho_1 - \rho_0)/\rho_0}$, with g being the gravitational acceleration and the scale length $H = L_2$. The quantities Re and Sc refer to the dimensionless Reynolds number $Re = U_b H/\nu$ and the Schmitd number $Sc = \nu/\kappa$, with ν being the kinematic viscosity and κ the mass diffusivity of the fluid ρ_1. $\hat{e}^g = (\sin\theta, -\cos\theta, 0)$ represent the direction of the gravitational acceleration, considering the bed slope angle θ. The slope of the domain occurs through the rotation of the axis-coordinates.

2.2 Numerical methodology

For the purpose to numerically solve the Equations 1, 2 and 3, the **Xcompact3D** code was used, based on the sixth-order compact finite difference scheme in spatial differentiation and temporal integration using the third-order Adams-Bashforth scheme. The pressure term is solved with Poisson's equation in spectral space using the fast Fourier transform.

The boundary conditions established in the problem for the velocity field on the x_1 and x_3 axis is free slip, in the case of the x_2 axis it is non-slip at $x_2 = 0$ and free slip at $x_2 = 1$. For the concentration field, the boundary conditions for x_1, x_2 and x_3 axes are zero flow.

The numerical simulation carried out in this work considers the dimensionless calculation domain $L_1 \times L_2 \times L_3 = (18 \times 1 \times 15)$, which is discretized into a Cartesian computational mesh with $721 \times 121 \times 601$ points, along the three main directions. The initial concentration is confined in the dimensionless cylindrical volume of radius $r_0 = 0.6$ and height $H = 1$, centered at the point $(x_1, x_3) = (4, 7.5)$. The bed slopes angles $\theta = [0°, 5°, 10°, 15°, 20°]$ are considered.

A time step equal to $\Delta t = 5 \times 10^{-4}$ is adopted, resulting in a final simulation time equal to 40 dimensionless units. The dimensionless numbers considered fit the simulations presented in Zgheib *et al.* (2016), which considered the Reynolds number $Re = 5000$ and the Schmidt number $Sc = 1$.

3. RESULTS

3.1 Front position and velocity

The gravity current propagation can be characterized by the front position of the current x_f, which is defined as the furthest point in the flow direction for each time step. The criteria adopted to track this position is $\varphi = 1 \times 10^{-2}$.

Figure 2 shows the influence of the bed slope. Initially ($t < 1.2$), the propagation is axisymmetric regardless of the bed slope. This suggests that the spreading in the early stages is similar to an expanding circle. After that, the spreading dynamics change depending on the bed slope.

In the plane case (zero bed slope), the front position of the gravity current shows monotonic spreading, contrasting with the sloping cases, which reveal an increase in spreading velocity.

At the final simulation times, the run-out of the gravity currents reaches the streamwise position $x_1 = 5.5$ and $x_1 = 13$, for $\theta = 0°$ and $\theta = 20°$, respectively. This suggests that the gravity current on the $20°$ slope travels ~ 2.4 times the distance compared to the plane slope case.

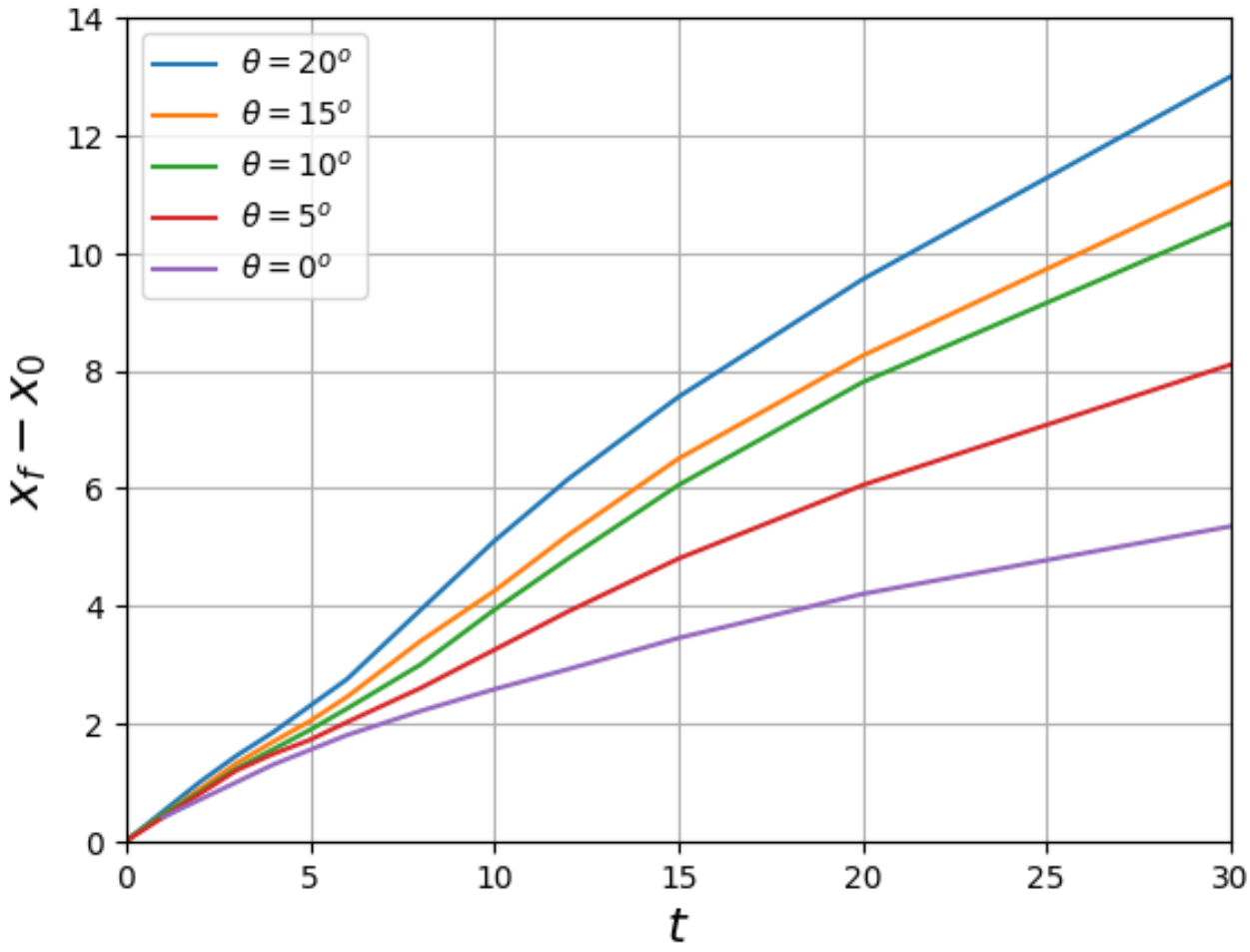

Figure 2. Temporal evolution of the front position, for all bed slope propagations.

To better understand the propagation dynamic of the gravity current is considered the front velocity v_f, which is obtained by differentiating with respect to time of the front position x_f, using a 4th order accurate centered scheme,

$$v_f = \frac{dx_f}{dt}. \tag{4}$$

Figure 3 shows the front velocity of the gravity currents, considering all slope cases, in comparison to the results obtained by Zgheib *et al.* (2016).

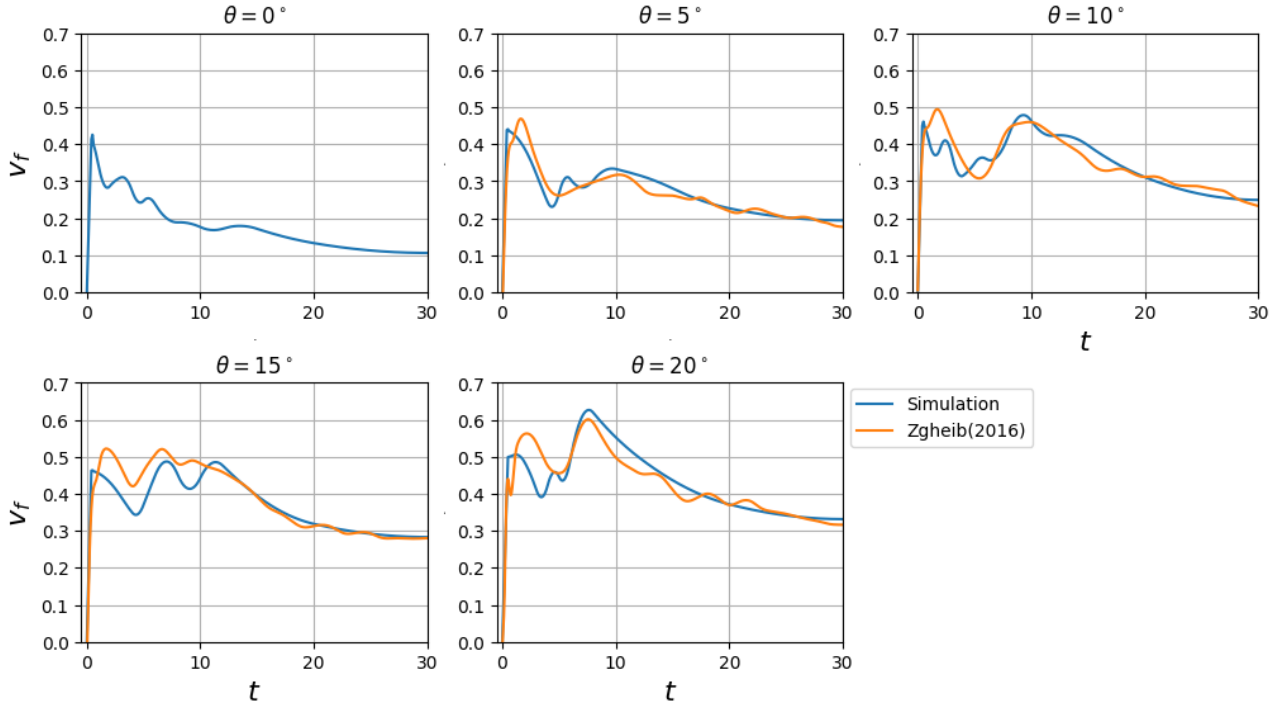

Figure 3. Temporal evolution of the front velocity, for all bed slope propagations.

In this figure, an initial acceleration regime is observed at early times for all slope cases. This is related to the formation of the gravity current. After this initial time instant ($t \approx 5$), the gravity current in the plane case reaches a constant velocity regime. This behavior is not observed in the cases with a bed slope. Instead, a second acceleration regime appear. This second acceleration regime was also reported by Zgheib *et al.* (2016), who showed that the second local maximum velocity increases with increasing slope and is even greater than the first local maximum for the steepest case. Later, around the time $t \approx 8$, the front velocities of the gravity currents decrease, transitioning to another regime. The deceleration rate is approximately the same for all cases of sloped bottoms. Therefore, at the end of the simulation, the current exhibits the highest velocity on the steepest slope.

3.2 Front Froude number

The bed slope has a strong influence on the current height, $\overline{h}$, which can be defined as:

$$\overline{h}(x_1, x_3, t) = \int_0^{L_2} \varphi(x_i, t) dx_2. \tag{5}$$

Fig. 4(a) shows the variation of the maximum current height over time as a function of the bottom slope. The figure reveals a relationship between periods of increased current height and second acceleration regime, once the gravity current is established. These heightened periods manifest as pulses whose duration increase with increasing bed slope. Notably, the current height for bed slopes of $\theta = 15°$ and $\theta = 20°$ exhibits distinct behavior compared to those at $\theta = 5°$ and $\theta = 10°$. In the plane slope case, the current height decrease after the acceleration regime, exhibiting a local maximum that could be related with the regime transitions described by the front velocity curve (Fig. 3).

From the front velocity, v_f (Eq. 4), and the maximum current height, $\overline{h}_{mx}$ (maximum value of the Eq. 5), it is possible to obtain the front Froude number, a dimensionless quantity that compares the inertial forces to gravitational forces in a fluid. It is defined as:

$$Fr = \frac{v_f}{(\overline{h}_{mx})^{1/2}}. \tag{6}$$

The Froude number can characterize the entrainment of ambient fluid into the gravity current. This entrainment affects both the density and velocity propagation of the current.

Figure 4 (b) shows the Froude number over time, for all bed slope cases.

For the bed slope cases, the figure reveals a stability time of $t \approx 8$, occurring after the second acceleration regime. This finding is consistent with the observations of Zgheib *et al.* (2016).

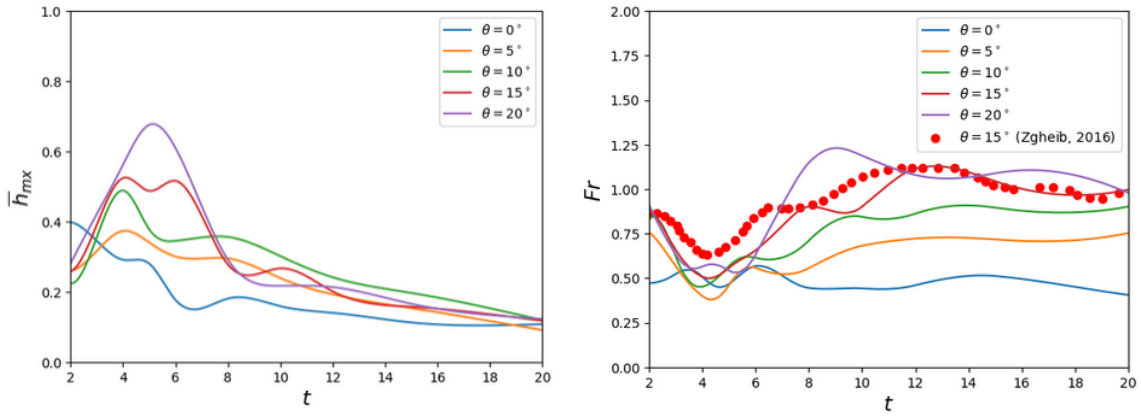

(a) (b)

Figure 4. Temporal evolution of the maximum value of current height (a) and the Froude number (b).

From the definition of the Froude number, it can be inferred that $Fr = 1$ represents a balance between inertial and gravitational forces. This value often corresponds to a transition point in the flow behavior.

Simulations reveal a distinct shift in the dominant forces governing gravity currents with increasing bed slope. For steeper slopes ($\theta = 15°$ and $\theta = 20°$), the Froude number, Fr, exceeds unity ($Fr > 1$), indicating supercritical flow driven by inertial forces. This dominance of inertial forces is likely due to the significant contribution of the slope to gravity current acceleration, stemming from the high initial potential energy in these cases. Conversely, for shallower slopes ($\theta = 0°$, $\theta = 5°$, and $\theta = 10°$), $Fr < 1$ (subcritical flow), signifying that gravitational forces exert primary control. This suggests that the current's hydrodynamic behavior in these cases more closely resembles that of a flat bottom.

3.3 Turbulent structures

At the beginning of the simulations, the gravity current is released from an initial volume, spreading radially. By time $t = 2$, the effect of the bed slopes becomes apparent, as evident in the x_3-component vorticity figure (Fig. 5), which reveals the breaking of the azimuthal symmetry. The plane case shows a symmetrical radial spreading, indicating that the current is uniform in all directions, while the sloping cases reveal a preferential spreading direction ($+x_1$). The height of the reverse current (the portion of the current attempting to propagate uphill in the $-x_1$ direction) decreases as the bed slope increases. Eventually, the reverse current stagnate and begins to propagate in the same preferential direction, mixing with the main current tail by the end of the simulation and contributing to the length of the current. This stagnation time depends on the bed slope, being longer for shallower slopes due to gravitational resistance and likely some viscous dissipation.

The head of the gravity current forms a rolled-up vortex tube that develops at early times ($t = 2$, $t = 3$ and $t = 4$) due to mixing at the interface between the gravity current and the surrounding fluid. During this process, the current height increases until the time $t = 5$, when the Kelvin-Helmholtz vortices collapse. The size of these large-scale vortex increases with increasing bed slope. The vortices collapse induces flow separation at the bottom of the domain due to an adverse pressure gradient. In the plane case and the lower bed slope ($\theta = 5°$ and $\theta = 10°$) cases, the separate current propagate back towards the initial release position, at least temporarily (in the lower bed slope). However, in the steeper cases ($\theta = 15°$ and $\theta = 20°$) the separated current continues to propagate in the preferential down-slope direction and mix with the main current. This process could justify the increase of the Froude number at time $t = 8$, causing the steepest cases into supercritical currents.

Figure 6 shows the Q-criterion methodology (Hunt *et al.*, 1988), that represents the positive part of the second invariant of the velocity gradient tensor. This definition allows the visualization of the three-dimensional structures typical of vortices. The figure shows that turbulence increases with increasing bed slope. At $t = 5$, for the steeper slope cases, vortex pairing is observed, with vortex tubes interconnecting. The steeper slopes, which lead to faster flow, may promote vortex pairing and contribute to the overall increase in turbulence intensity.

In the plane case, at $t = 8$, hairpin vortices develop, potentially contributing to the formation of lobes and clefts that become clearly visible by $t = 10$.

For the steeper cases, the front of the current assumes an elongated shape, particularly at times associated with the deceleration regime, after $t > 8$.

In Fig. 6, due to the appearance of the turbulent structures of the density current, the formation of a hydraulic jump (characterizing the transition from a supercritical to a subcritical regime) can be observed for slopes greater than $\theta = 5°$.

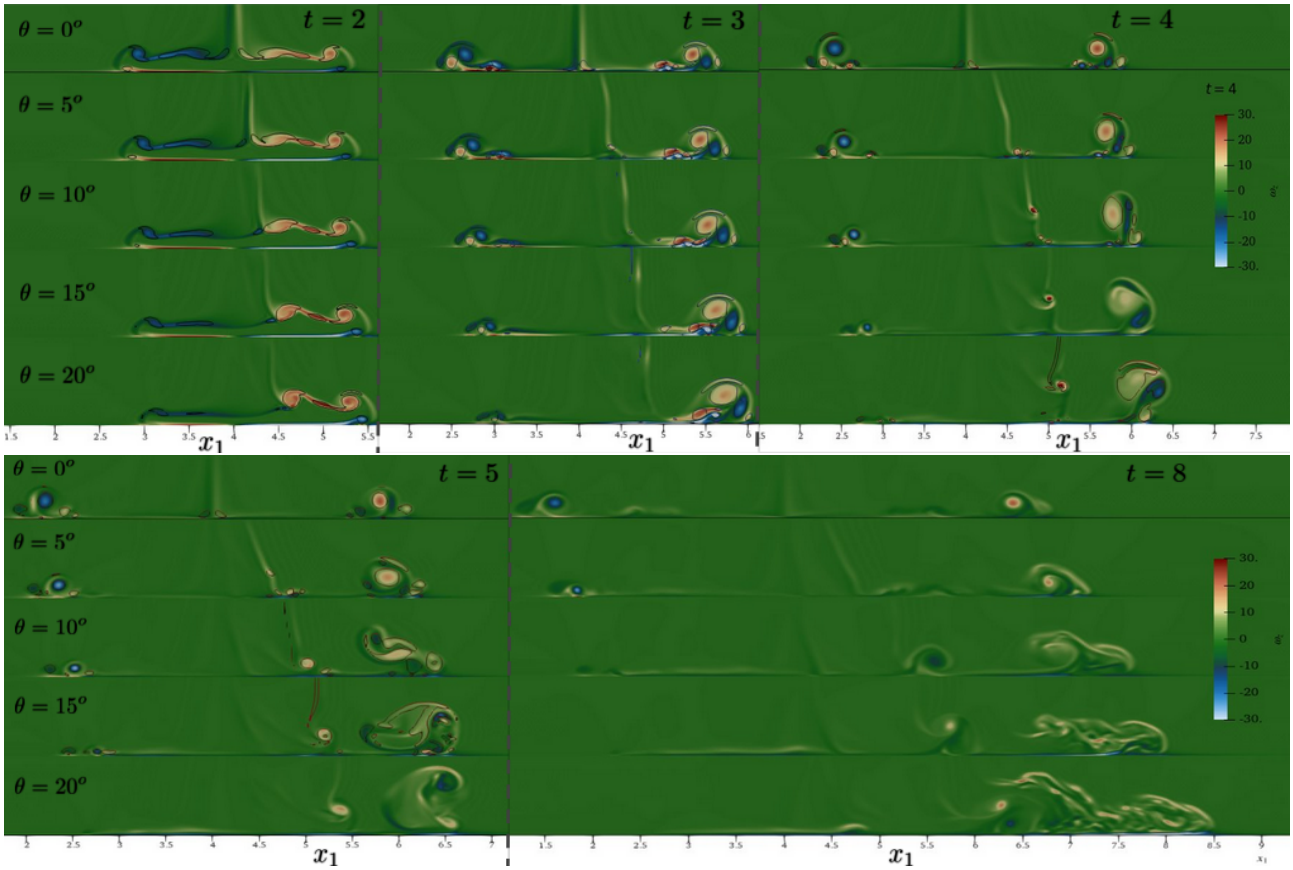

Figure 5. z-component vorticity, for $t = [2, 3, 4, 5, 8]$

On slopes less than 10º, the hydraulic jump formed presents a more radial behavior, while on greater slopes it tends to present a greater intensity and influence in the streamwise direction.

Evidently, the Froude number based on the velocity of the current front and its maximum height cannot be applied to characterize the hydrodynamics of the hydraulic jump formed, nor its probable conjugate heights, since the Froude number presented in Fig. 4(b) only presents values greater than 1 for slopes greater than $\theta = 15°$. On the other hand, it is observed that current front Froude numbers greater than 1 are associated with those hydraulic jumps of greater intensity, turbulent and more concentrated in the streamwise direction, demonstrating a greater similarity with the jumps observed in classical cases of free surface flows. These results also demonstrate the importance of a more in-depth study on this subject, representing a gap to be filled by future work.

4. CONCLUSIONS

Numerical simulations were performed to evaluate the gravity current spreading of cylindrical lock release, under the influence of the bed slope. The Reynolds number $Re = 5000$ and the bed slope of variations $\theta = [0°, 5°, 10°, 15°, 20°]$ were considered, in concordance with Zgheib *et al.* (2016), except for the plane slope case.

The front velocities found in this work agree with the reference, as was shown in the Fig. 3. The bed slope influences the propagation dynamics of the density current, adding a second acceleration regime after the current formation. This regime could be related to the height current increases, whose duration depends on the bed slope.

The study also reveals that bed slope significantly influences the evolution, and turbulence, of gravity currents. While a plane surface allows for symmetrical radial spreading, the presence of a slope introduces a preferential downslope propagation, inhibiting the uphill flow of the reverse current. This reverse current eventually stagnates and merges with the main current, with the stagnation time being longer for shallower slopes due to increased gravitational resistance.

The formation and evolution of vortex structures are also notably impacted by the bed slope. For all cases, a rolled-up vortex tube develops at the head of the current, with its size increasing with steeper slopes. The collapse of these vortices induces flow separation, which exhibits distinct behavior depending on the slope. In shallower slopes, the separated current tends to reverse direction, while in steeper cases, it continues downslope, potentially contributing to an increase in the Froude number and the development of supercritical flow.

Furthermore, steeper slopes are linked to increased turbulence intensity, characterized by vortex pairing and the formation of interconnected vortex tubes. Hairpin vortices emerge, potentially leading to the development of lobes and clefts

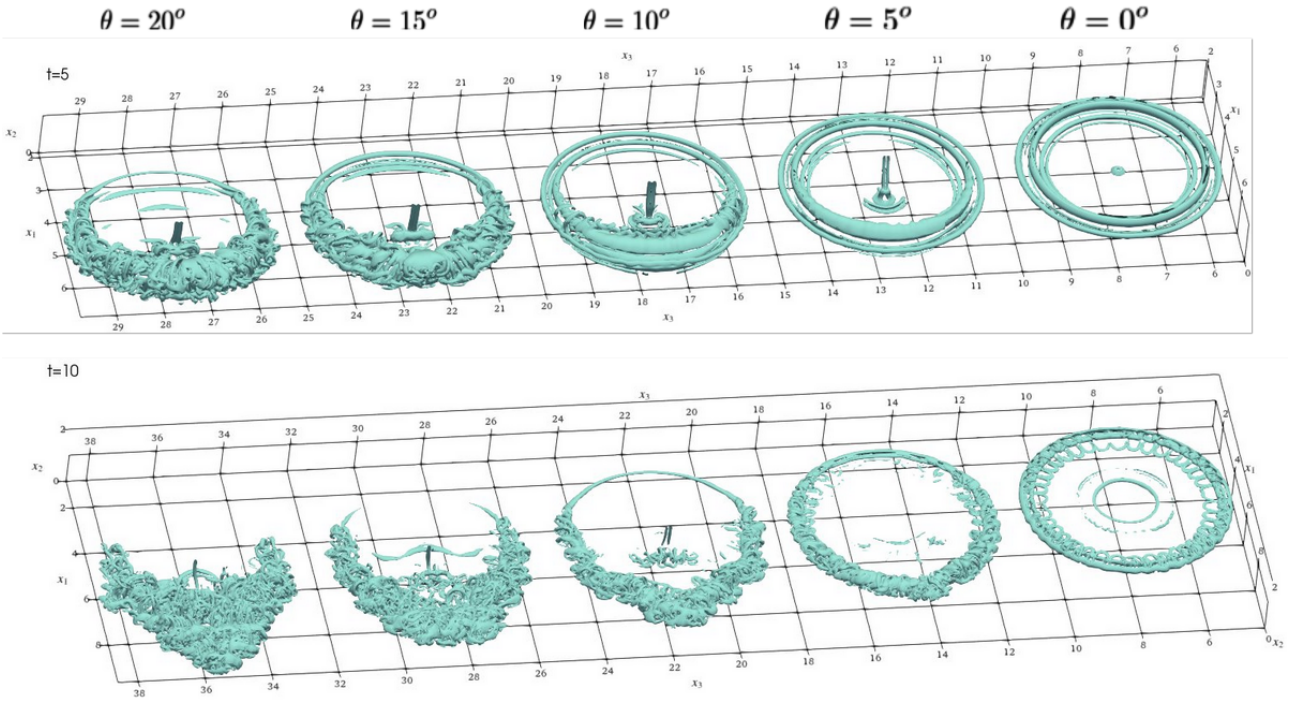

Figure 6. Q-criterion isocontour of $Q = 1$, at the times $t = 5$ and $t = 10$.

in the current. These findings underscore the crucial role of bed slope in shaping the complex interplay of forces, mixing processes, and energy cascades within gravity currents.

The analysis of turbulent structures in Fig. 6 reveals a complex relationship between hydraulic jump formation and bed slope in density currents. While visual evidence suggests hydraulic jumps occur at slopes greater than $\theta = 5°$, the Froude number, calculated using front velocity and maximum height, only indicates supercritical flow (characteristic of intense jumps) for slopes exceeding $\theta = 15°$. This discrepancy highlights the limitations of applying traditional Froude number analysis to density currents on slopes. This research emphasizes the need for a more nuanced understanding of hydraulic jumps in density currents, moving beyond traditional methods to accurately characterize and predict their behavior across varying slopes.

5. ACKNOWLEDGEMENTS

The Authors would like to thank the PUCRS High Performance Laboratory (LAD) for providing the supercomputer resources for the results of the numerical simulations reported in this study. The authors thank Petrobras for financing this research.

6. REFERENCES

Azpiroz-Zabala, M., Cartigny, M.J., Talling, P.J., Parsons, D.R., Sumner, E.J., Clare, M.A., Simmons, S.M., Cooper, C. and Pope, E.L., 2017. "Newly recognized turbidity current structure can explain prolonged flushing of submarine canyons". *Science advances*, Vol. 3, No. 10, p. e1700200.

Bonnecaze, R.T., Hallworth, M.A., Huppert, H.E. and Lister, J.R., 1995. "Axisymmetric particle-driven gravity currents". *J. Fluid Mech.*, Vol. 294, pp. 93–121.

Cantero, M.I., Lee, J.R., Balachandar, S. and García, M.H., 2007. "On the front velocity of gravity currents". *J. Fluid Mech.*, Vol. 586, pp. 1–39.

Cantero, M.I., Balachandar, S., García, M.H. and Bock, D., 2008. "Turbulent structures in planar gravity currents and their influence on the flow dynamics". *Journal of Geophysical Research: Oceans*, Vol. 113, No. C8.

Dai, A. and Huang, Y.L., 2022. "On the merging and splitting processes in the lobe-and-cleft structure at a gravity current head". *Journal of Fluid Mechanics*, Vol. 930, p. A6. doi:10.1017/jfm.2021.906.

Dorrell, R.M., Burns, A.D. and McCaffrey, W.D., 2015. "The inherent instability of leveed seafloor channels". *Geophysical Research Letters*, Vol. 42, No. 10, pp. 4023–4031.

Dubief, Y. and Delcayre, F., 2000. "On coherent-vortex identification in turbulence." *Journal of Turbulence.*, p. N11.

Espath, L.F.R., Pinto, L.C., Laizet, S. and Silvestrini, J.H., 2015. "High-fidelity simulations of the lobe-and-cleft structures and the deposition map in particle-driven gravity currents". *Physics of Fluids*, Vol. 27, No. 5, p. 056604.

Farenzena, B.A., 2021. "Relatório final de pós-doutorado: O alcance de correntes de turbidez". Technical report. Post-doctoral Report.

Francisco, E.P., Espath, L.F.R., Laizet, S. and Silvestrini, J.H., 2017. "Direct numerical simulation of bi-disperse particle-laden gravity currents in the channel configuration". *Applied Mathematical Modelling*, Vol. 49, pp. 739–752.

Frantz, R.A., Deskos, G., Laizet, S. and Silvestrini, J.H., 2021. "High-fidelity simulations of gravity currents using a high-order finite-difference spectral vanishing viscosity approach". *Computers & Fluids*, Vol. 221, p. 104902. ISSN 0045-7930. doi:https://doi.org/10.1016/j.compfluid.2021.104902.

Härtel, C., Meiburg, E. and Necker, F., 2000. "Analysis and direct numerical simulation of the flow at a gravity-current head. part 1. flow topology and front speed for slip and no-slip boundaries". *Journal of Fluid Mechanics*, Vol. 418, pp. 189–212.

Hunt, J.C.R., Wray, A.A. and Moin, P., 1988. "Eddies, streams, and convergence zones in turbulent flows". URL https://api.semanticscholar.org/CorpusID:35721045.

Kneller, B.C., Bennett, S.J. and McCaffrey, W.D., 1999. "Velocity structure, turbulence and fluid stresses in experimental gravity currents". *Journal of Geophysical Research*, Vol. 104, No. C3, pp. 5381–5391.

Kuenen, P.H. and Menard, H.W., 1952. "Turbidity currents, graded and non-graded deposits". *Journal of Sedimentary Research*, Vol. 22, No. 2.

Mulder, T. and Alexander, J., 2001. "The physical character of subaqueous sedimentary density flows and their deposits". *Sedimentology*, Vol. 48, No. 2, pp. 269–299.

Ross, A.N., Linden, P.F. and Dalziel, S.B., 2002. "A study of three-dimensional gravity currents on a uniform slope". *Journal of Fluid Mechanics*, Vol. 453, pp. 239 – 261. URL https://api.semanticscholar.org/CorpusID:1043967.

Schuch, F.N., Pinto, L.C., Silvestrini, J.H. and Laizet, S., 2018. "Three-dimensional turbulence-resolving simulations of the plunge phenomenon in a tilted channel". *Journal of Geophysical Research: Oceans*, Vol. 123, No. 7, pp. 4820–4832.

Simpson, J.E., 1999. *Gravity currents: In the environment and the laboratory*. Cambridge university press.

Sylvester, Z., Pirmez, C. and Cantelli, A., 2011. "A model of submarine channel-levee evolution based on channel trajectories: Implications for stratigraphic architecture". *Marine and Petroleum Geology*, Vol. 28, No. 3, pp. 716–727. ISSN 0264-8172. doi:https://doi.org/10.1016/j.marpetgeo.2010.05.012. URL https://www.sciencedirect.com/science/article/pii/S0264817210001157. Thematic Set on STRATIGRAPHIC EVOLUTION OF DEEP-WATER ARCHITECTURE.

Talling, P.J., Allin, J., Armitage, D.A., Arnott, R.W.C., Cartigny, M.J.B., Clare, M.A., Felletti, F., Covault, J.A., Girardclos, S., Hansen, E. *et al.*, 2015. "Key future directions for research on turbidity currents and their deposits". *Journal of Sedimentary Research*, Vol. 85, No. 2, pp. 153–169.

Vianna, F., Farenzena, B., Pinho, M. and Silvestrini, J., 2022. "Spatiotemporal flow features in gravity currents using computer vision methods". *Computers Geosciences*, Vol. 165, p. 105146. ISSN 0098-3004. doi:https://doi.org/10.1016/j.cageo.2022.105146. URL https://www.sciencedirect.com/science/article/pii/S0098300422001017.

Zgheib, N., Ooi, A. and Balachandar, S., 2016. "Front dynamics and entrainment of finite circular gravity currents on an unbounded uniform slope". *Journal of fluid mechanics*, Vol. 801, pp. 322–352. doi:https://doi.org/10.1017/jfm.2016.325. URL https://doi.org/10.1017/jfm.2016.325.

7. RESPONSIBILITY NOTICE

The authors are the only responsible for the printed material included in this paper.